Contents lists available at ScienceDirect

Journal of Biomechanics

ELSEVIER

Effect of side branch flow upon physiological indices in coronary artery disease

Rebecca C. Gosling [a,b,c,1], Jacob Sturdy [d,1,*], Paul D. Morris [a,b,c], Fredrik Eikeland Fossan [d], Leif Rune Hellevik [d], Patricia Lawford [a,b], D. Rodney Hose [a,b,e], Julian Gunn [a,b,c]

[a] Department of Infection, Immunity and Cardiovascular Disease, The University of Sheffield, Sheffield, UK
[b] Insigneo Institute for In-silico Medicine, Sheffield, UK
[c] Department of Cardiology, Sheffield Teaching Hospitals NHS Foundation Trust, Sheffield, UK
[d] Department of Structural Engineering, Norwegian University of Science and Technology, Trondheim, Norway
[e] Department of Circulation and Medical Imaging, Norwegian University of Science and Technology, Trondheim, Norway

ARTICLE INFO

ABSTRACT

Recent efforts have demonstrated the ability of computational models to predict fractional flow reserve from coronary artery imaging without the need for invasive instrumentation. However, these models include only larger coronary arteries as smaller side branches cannot be resolved and are therefore neglected. The goal of this study was to evaluate the impact of neglecting the flow to these side branches when computing angiography-derived fractional flow reserve (vFFR) and indices of volumetric coronary artery blood flow. To compensate for the flow to side branches, a leakage function based upon vessel taper (Murray's Law) was added to a previously developed computational model of coronary blood flow. The augmented model with a leakage function ($1D_{leaky}$) and the original model (1D) were then applied to predict FFR as well as inlet and outlet flow in 146 arteries from 80 patients who underwent invasive coronary angiography and FFR measurement. The results show that the leakage function did not significantly change the vFFR but did significantly impact the estimated volumetric flow rate and predicted coronary flow reserve. As both procedures achieved similar predictive accuracy of vFFR despite large differences in coronary blood flow, these results suggest careful consideration of the application of this index for quantitatively assessing flow.

1. Introduction

Fractional flow reserve (FFR) is the gold standard method to evaluate the physiological significance of epicardial coronary artery disease (CAD) (Neumann et al., 2018). Yet, clinical uptake is poor due to availability, time constraints, and the invasive nature of the procedure (Dehmer et al., 2012). Several groups have evaluated computational fluid dynamics (CFD) methods to compute FFR

and achieved relatively high diagnostic accuracy (FFR $\leq$ or > 0.80) (Gosling et al., 2019; Koo et al., 2011; Min et al., 2012; Morris et al., 2013; Nakazato et al., 2013; Papafaklis et al., 2014; Tu et al., 2014; Norgaard et al., 2014). Quantitative accuracy, however, remains limited (Morris et al., 2015, 2020). Accuracy is limited by various anatomical and physiological assumptions made to enable computational modelling (Eck et al., 2016; Fossan et al., 2018; Morris et al., 2017; Sankaran et al., 2016; Sturdy et al., 2019). When constructing a geometric model of the coronary arteries, assumptions must be made about which branches and outlets should be represented explicitly. Prior work often assumes the flow to side branches is non-influential and models the artery of interest as a single lumen (Morris et al., 2013). To a degree, all approaches neglect some side branches due to limitations in medical imaging, even if some approaches model all the larger side-branches seen in the medical images (Blanco et al., 2018; Fossan et al., 2018; Koo et al., 2011). Tu et al. (2016) implicitly accounted for flow to side branches by assuming constant flow velocity; however, no

comparison was made to evaluate the impact of this assumption. This study seeks to quantify the effect of neglecting side branch flow when predicting FFR and other indices of coronary physiology.

Whilst geometric modelling of side-branches is impractical, it is possible to compensate for the flow to neglected branches by means of a leakage function, which quantifies the flow leaving the main vessel along its length. An estimate of the flow to these branches may be derived from Murray's law, which relates changes in vessel calibre (taper) to blood flow and shear stress (Murray, 1926). This study augmented a model for FFR prediction (Fossan et al., 2018) with a leakage function and applied both models to predict FFR and volumetric flow in 146 arteries from patients with CAD.

2. Methods

2.1. Study population

Data were collected prospectively from patients with stable coronary artery disease undergoing invasive coronary angiography. Patients were excluded if they had presented acutely within the previous 60 days, had previous coronary artery bypass graft surgery or chronic total occlusions, or were unable to provide consent.

2.2. Procedural protocol

Patients underwent invasive coronary angiography using standard techniques. All arteries with disease affecting >50% diameter were assessed with a pressure wire (Philips/ Volcano Primewire or PressureWire™ X guidewire, St Jude/Abbott). FFR was measured in diseased vessels during maximal stable hyperaemia (Sciola et al., 2018) induced by intravenous infusion of adenosine (140 µg/kg/min).

2.3. Vessel segmentation and reconstruction

3D vessel anatomy was reconstructed with outlet corresponding to the location where distal pressure was measured from two 2D angiographic acquisitions and the segments of interest were extracted as a single lumen model via purpose built software.

2.4. 1D model

Radius data were sampled with a spacing of 0.1 mm along the centreline of the reconstructed vessel to produce a 1D axisymmetric model of each vessel (see Fig. 1). Volumetric flow and virtual FFR (vFFR) were computed with a 1D model (Fossan et al., 2018) derived from the Navier-Stokes equations under assumptions of axial-symmetry and steady, laminar flow, which closely approximate full 3D simulations of blood flow (Alastruey et al., 2016; Blanco et al., 2018; Boileau et al., 2015; Fossan et al., 2018).

For this model the pressure difference between two points x_i and x_{i+1} on the centreline of the artery is

$$P_i - P_{i+1} = \rho \frac{1}{2}\left(\frac{Q_{i+1}}{A_{i+1}}\right)^2 - \rho \frac{1}{2}\left(\frac{Q_i}{A_i}\right)^2 + \int_0^l Q \frac{2(\zeta+2)\pi\mu}{A^2}dx \quad (1.1)$$

where P is pressure, Q volumetric flow, and A cross sectional area. The parameter ζ is related the assumption that the velocity profile in the vessel is

$$v(R) = \frac{Q}{A}\frac{\zeta+2}{\zeta}\left[1 - \left(\frac{\sqrt{\pi}R}{\sqrt{A}}\right)^\zeta\right] \quad (1.2)$$

where R is the radial coordinate. Fossan et al. (2018) found that $\zeta = 4.31$ gives good agreement with 3D CFD in coronary arter-

ies. The values of viscosity and blood density were $\mu = 3.5e - 3$ Pa s and $\rho = 1050$ kg/m^3.

Abrupt changes in geometry at stenoses invalidate the assumptions of this model, thus the pressure drop across a stenosis is modelled by an experimentally derived pressure loss term:

$$\Delta P = \frac{K_v \mu}{A_0 D_0}Q + \frac{K_t \rho}{2A_0^2}\left(\frac{A_0}{A_s}-1\right)^2 Q|Q|, \quad (1.3)$$

where A_0 and A_s refer to the cross-sectional areas of the normal and stenotic segments, respectively. Similarly, D_0 and D_s represent the normal and stenotic diameters and L_s the length of the stenosis. K_v and K_t are empirical coefficients, with $K_v = 32(0.83L_s + 1.64D_s) \cdot (A_0/A_s)^2/D_0$ and $K_t = 1.52$ (Liang et al., 2011).

To determine exactly where the stenosis model should be applied, a stenosis detection filter was used to identify stenotic regions based on an estimated "healthy" radius of the vessel as described previously (Fossan et al., 2018). The stenosis model is applied when the degree of vessel narrowing exceeds a threshold.

2.5. Leakage model

Because the reconstructed anatomy neglects side branches, the assumption that inflow equals outflow ($Q_{in} = Q_{out}$) in the main vessel is invalid. To extend the 1D model, the flow Q in (1.1) is varied along the centreline to account for flow to branches which are not explicitly represented. The relative proportion of flow to side branches is predicted according to Murray's law, which posits that the radii (r) of blood vessels are adapted to achieve an equipoise between flow (Q) and energy expenditure (Murray, 1926)

$$Q \propto r^c \quad (1.4)$$

where the exponent c depends upon the energetic costs. Experimental and theoretical considerations require that $2.33 \leq c \leq 3$. The value $c = 2.4$ was used as a preliminary analysis indicated that altering the value of c did not significantly change the results (see supplemental Table 1).

Murray's law implies that tapering of an arterial segment corresponds to the amount of flow to branches, and thus the flow to such arteries may be estimated from Eq. (1.4), which implies that the ratio of flow at the inlet and outlet of the segment is:

$$\frac{Q(0)}{Q(L)} = \left(\frac{r(0)}{r(L)}\right)^c \quad (1.5)$$

where (0) indicates the inlet and (L) the outlet of the vessel. Furthermore, if the branches are assumed to be uniformly distributed along the length of the segment, the flow can be determined at any position (x) along the segment:

$$Q(x) = \left[\frac{r(0) - \frac{r(0)-r(L)}{L}x}{r(0)}\right]^c Q(0). \quad (1.6)$$

To formulate the 1D$_{leaky}$ model, (1.6) is substituted into (1.1) accounting for flow to side branches inferred from the geometric taper of the vessel and Murray's law:

$$P_i - P_{i+1} = \rho \frac{1}{2}\left(\frac{Q(x_{i+1})}{A_{i+1}}\right)^2 - \rho \frac{1}{2}\left(\frac{Q(x_i)}{A_i}\right)^2 + \int_0^l Q(x)\frac{2(\zeta+2)\pi\mu}{A^2}dx \quad (1.7)$$

In practice the radius r(x) observed from the angiogram may be diseased and thus deviate from Murray's law, hence an estimate of the healthy radius is used in (1.6) to determine the flow to side branches. This estimate of the healthy radius is identical to that used in the stenosis detection filter. Further, in some cases -even with this smoothing- the inlet radius is larger than the outlet radius. For these cases, no flow is distributed to side branches as

Reconstruct 3D geometry from angiography data
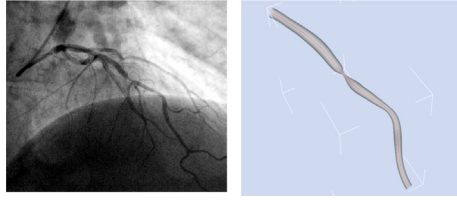
Extract radius from 3D-reconstruction to generate 1D domain.
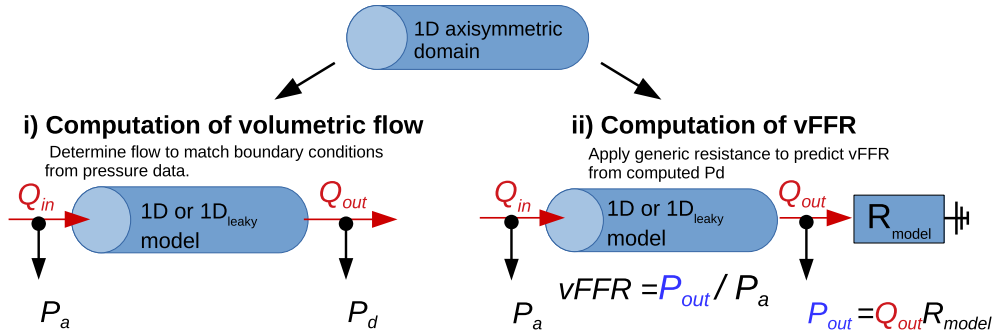
Fig. 1. Illustration of computational workflow, The above figure illustrates the computational workflow beginning with geometric reconstruction from the angiographic images (top) and subsequent construction of a 1D axisymmetric geometric model of each vessel (middle row). Finally, the two distinct boundary conditions applied to both the 1D and 1Dleaky to compute (i) the volumetric flow and (ii) virtual FFR are depicted (bottom row).

(1.6) would suggest an unphysiological mass influx from side branches. Thus if r(L) > r(0) the 1Dleaky model is identical to the 1D model.

2.6. Boundary conditions and analysis protocol

Fig. 1 illustrates the computational analysis of both 1D and 1Dleaky models. For each model one simulation is performed to compare the volumetric hyperaemic flow and associated indices and another is performed to quantify vFFR's accuracy. First, measured inlet and outlet pressures are imposed to determine each model's predicted volumetric flow. Second, to predict vFFR, measured inlet pressure is applied while a generic distal resistance is applied at the outlet.

(i) Pressure matching computation of volumetric flow

To compute the volumetric flow, the invasively measured proximal (P_a) and distal (P_d) pressures were applied at the inlet and outlet respectively. The corresponding volumetric flow (Q) was then determined computationally (See Fig. 1), and used to calculate coronary microvascular resistance (CMVR) and stenotic segment resistance (SR):

$$CMVR = \frac{P_d}{Q_{out}} \qquad (1.8)$$

$$SR = \frac{P_a - P_d}{1/2(Q_{in} + Q_{out})}$$

(ii) Minimally invasive prediction of vFFR

vFFR offers a less-invasive alternative to FFR and avoids passage of a pressure wire. The proximal boundary is set to match the patient-specific mean proximal (aortic) pressure (Pa). This is easily measured during any catheterization procedure (diagnostic or PCI). The distal boundary represents the distal CMVR, which is unknown and thus more challenging. In this study a model-specific resistance (R_{model}) is applied as the distal boundary condition such that $P_{out} = R_{model}Q_{out}$ (see Fig. 1). The value of R_{model} is the average of all CMVR values calculated from the volumetric flow in setting (i) for the given model (1D = 1.23e+10 Pa/m^3 s^{-1} and 1Dleaky = 2.42e

+10 Pa/m^3 s^{-1}). vFFR is calculated from the outlet pressure (P_{out}) computed for the given aortic pressure (P_a) and resistance (R_{model}):

$$vFFR = \frac{P_{out}}{P_a}. \qquad (1.9)$$

2.7. Computation of baseline flow and coronary flow reserve

The focus of this study was computation of hyperaemic flow and prediction of FFR; however, the flow under resting conditions is also of interest, and the ratio of flow between resting and maximal hyperaemic conditions defines the coronary flow reserve (CFR), the extent to which coronary flow may be increased to meet physiological demands.

To compute baseline volumetric flow for each model, the measured inlet and outlet pressures were imposed and the flow generating a matching pressure drop was determined, in the same manner as for the hyperaemic state. Then, combining baseline and hyperaemic flow estimates, CFR may be predicted as

$$CFR = Q_{in}^{hyp}/Q_{in}^{bl}$$

where Q_{in}^{bl} is the flow determined from matching the baseline pressures and, Q_{in}^{hyp}, is the flow determined from matching the hyperaemic pressures.

A virtual CFR (vCFR) that could be computed from minimally invasive measurements was computed in a similar manner to vFFR, where a generic baseline CMVR is applied as a distal boundary condition to predict baseline flow. Then ratio of flows computed using hyperaemic CMVR and baseline CMVR may be used to compute vCFR as

$$vCFR = \tilde{Q}_{in}^{hyp}/\tilde{Q}_{in}^{bl} \qquad (1.9$$

where $\tilde{Q}_{in}^{bl}$ is the flow determined by applying the measured baseline inlet pressure and the generic baseline CMVR (1D = 2.83e+10 Pa/m^3 s^{-1} and 1Dleaky = 5.95e+10 Pa/m^3 s^{-1}) at the outlet, and

$\tilde{Q}_{in}^{hyp}$ is the flow determined by applying the measured hyperaemic inlet pressure and generic hyperaemic CMVR at the outlet.

2.8. Statistical analysis

Data are presented as median and 25th and 75th percentiles unless stated otherwise. Tables 4 and 5 summarize quantitative results. Differences between models were analysed with robust linear regression with a two-sided test for non-zero differences using the Python library statsmodels (Seabold and Perktold, 2010) as the Shaprio-Wilk test indicated differences were not normally distributed. Differences between the bias (vFFR – FFR), absolute error (|vFFR – FFR|), inflows, outflows, and resistances were analysed identically. Diagnostic accuracy was assessed by sensitivity, specificity, positive predictive value, negative predictive value and overall accuracy on dichotomised data (FFR > or $\leq$ 0.80). Bland-Altman analyses compared FFR and vFFR of each model (see Fig. 2B–D).

3. Results

Tables 1–4 present the summary statistics of all quantities of interest that are presented in the following paragraphs.

3.1. Patient and lesion characteristics

Eighty patients with angiographically confirmed coronary artery disease were studied. Table 1 shows baseline patient and lesion characteristics. The mean age was 65.8 ± 10.2(std. dev.) years. 25% of patients were male, 20% had type 2 diabetes mellitus, and 10% were current smokers. 146 arteries were studied; 84 left anterior descending (LAD), 29 left circumflex (LCX), 31 right coronary (RCA) and 2 intermediate arteries. Median invasively

Table 1
Patient and lesion characteristics.

Patient characteristics (N = 80)	
Age	65.8 (10.2)
Male	20 (25%)
Current smoker	8 (10%)
T2DM	16 (20%)
Hyperlipidaemia	59 (74%)
Previous MI	30 (38%)
Lesion characteristics (N = 146)	
Average % diameter stenosis	58.6 (15.4)
SYNTAX score	11.5 (6.7)
Artery	84-LAD, 29-LCX, 31-RCA, 2-IM
Ratio of inlet diameter to outlet	0.65 ± 0.220.62 ± 0.17 in LAD vs 0.69 ± 0.27 otherwise
Artery length	77.7 ± 27.1 mm78.3 ± 24.5 in LAD vs 76.7 ± 30.5 otherwise
Invasive FFR	0.80 (±0.14), 43 in the range 0.75–0.85

measured FFR was 0.834(0.736–0.901) with 43 (29%) within the range 0.75–0.85. The median length of vessels studied was 73.0 mm (59.6–95.5).

3.2. FFR computation

Median vFFR for the 1D and 1D$_{leaky}$ models were 0.91(0.82–0.95) and 0.92(0.81–0.96) respectively (see Fig. 2A for a scatter plot of vFFR for each modes). Including leakage increased vFFR by an average of 0.005 (95%CI 0.0, 0.01; p = 0.08).

3.3. Quantitative and diagnostic accuracy

Overall diagnostic accuracy (ability to predict FFR $\leq$ or > 0.80) was similar for both models (1D 75%; 1D$_{leaky}$ 72%) as were other
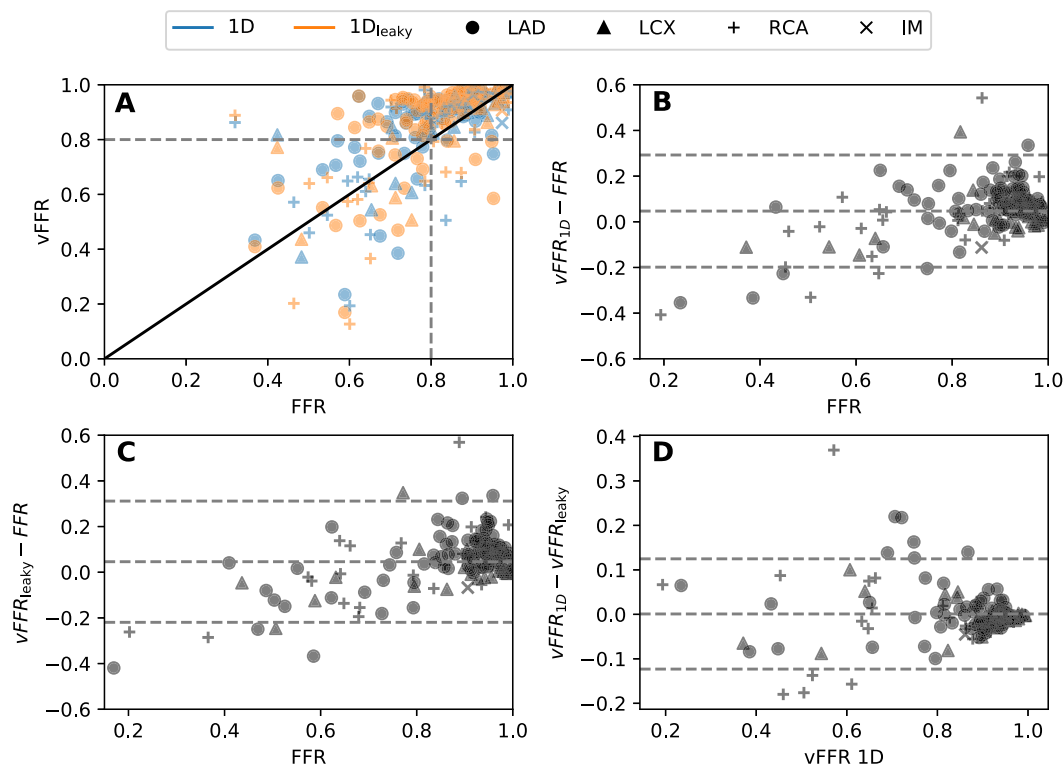
Fig. 2. Comparison of FFR and vFFR, A scatter plot (A) of vFFR vs FFR for all cases. The markers indicate the anatomical branch of the case, and the black line represents where vFFR equals FFR. Dashed lines indicate the clinical cut-off value of 0.8 for determining the significance of CAD. The correlation coefficient between 1D vFFR and FFR was 0.65, between 1Dleaky vFFR and FFR was 0.65, and between 1D and 1Dleaky vFFR was 0.93. Bland-Altman plots for 1D model (B) and 1D$_{leaky}$ model (C) and between models (D). Limits of agreements are −0.22–0.31, −0.20–0.29 and −0.12–0.12, respectively with mean biases of −0.046, −0.047, and 0.001 respectively.

Table 2
Comparison of diagnostic and uantitative accuracy of vFFR models.

	Diagnostic accuracy	Sensitivity	Specificity	PPV	NPV
1D	75%	46%	95%	88%	71%
$1D_{leaky}$	72%	46%	91%	78%	70%
	Mean vFFR	**Mean bias (FFR-vFFR)**	**AUC**	**Correlation**	**Average error |FFR-vFFR|**
1D	0.85(0.16)	−0.05(0.13)	0.84	0.65	0.10(0.09)
$1D_{leaky}$	0.85(0.18)	−0.05(0.14)	0.82	0.65	0.11(0.10)

Table 3
Summary statistics (mean, standard deviation, median, 25th percentile and 75th percentile) of FFR and vFFR related quantities for both 1D and $1D_{leaky}$ models.

		mean	std	median	25%	75%
Invasive FFR	**All**	0.803	0.138	0.834	0.736	0.901
	LAD	0.795	0.118	0.818	0.740	0.877
	LCX	0.863	0.146	0.901	0.832	0.965
	RCA	0.757	0.164	0.798	0.644	0.879
Lengths	**All**	77.667	27.104	72.952	59.580	95.511
	LAD	78.333	24.455	72.316	62.466	93.756
	LCX	64.353	19.552	66.640	54.150	74.353
	RCA	91.245	32.029	95.477	74.997	105.732
vFFR	**1D vFFR**	0.850	0.159	0.911	0.816	0.947
	$1D_{leaky}$ vFFR	0.849	0.175	0.923	0.808	0.957
	$1D_{leaky}$ vFFR − 1D vFFR	−0.001	0.063	0.007	−0.012	0.020
	1D Bias	0.047	0.126	0.056	−0.003	0.103
	$1D_{leaky}$ Bias	0.046	0.136	0.066	−0.004	0.115
	|1D vFFR - FFR|	0.099	0.090	0.079	0.040	0.133
	|$1D_{leaky}$ vFFR − FFR|	0.107	0.095	0.083	0.039	0.138
vFFR LAD	**1D vFFR**	0.867	0.137	0.913	0.846	0.944
	$1D_{leaky}$ vFFR	0.861	0.156	0.923	0.847	0.949
	$1D_{leaky}$ vFFR − 1D vFFR	−0.007	0.055	0.004	−0.014	0.015
	1D Bias	0.072	0.110	0.082	0.041	0.131
	$1D_{leaky}$ Bias	0.065	0.125	0.080	0.024	0.130
	|1D vFFR - FFR|	0.108	0.075	0.094	0.053	0.141
	|$1D_{leaky}$ vFFR − FFR|	0.113	0.083	0.089	0.058	0.146

Table 4
Summary statistics (mean, standard deviation, median, 25th percentile and 75th percentile) of flow and resistance related quantities.

|		mean	std	median	25%	75%
Hyperaemic Flows	**1D flow**	1.534	1.162	1.257	0.734	2.034
	$1D_{leaky}$ inflow	2.523	2.126	1.974	1.134	3.452
	Inflow ratio ($1D_{leaky}$:1D)	1.664	0.629	1.479	1.249	1.895
	$1D_{leaky}$ outflow	1.001	0.986	0.752	0.360	1.351
	Outflow ratio ($1D_{leaky}$:1D)	0.620	0.212	0.601	0.468	0.769
	Leaked flow	1.522	1.710	1.090	0.399	2.091
	Pct flow leaked	56%	26%	63%	44%	74%
	LAD Pct flow leaked	60%	23%	67%	48%	74%
	LCX Pct flow leaked	56%	30%	67%	45%	80%
	RCA Pct flow leaked	44%	29%	47%	24%	70%
Baseline flows and CFR	**1D flow**	0.826	0.658	0.638	0.305	1.235
	$1D_{leaky}$ inflow	1.346	1.094	1.049	0.495	1.938
	1D CFR	2.236	1.277	1.922	1.543	2.592
	$1D_{leaky}$ CFR	2.248	1.286	1.919	1.537	2.621
	1D vCFR	2.616	0.439	2.739	2.362	2.931
	$1D_{leaky}$ vCFR	2.753	0.492	2.907	2.417	3.095
Hyperaemic CMVR	**1D**	1.22E + 10	1.52E + 10	6.928E + 09	4.49E + 09	1.25E + 10
	$1D_{leaky}$	2.35E + 10	3.58E + 10	1.253E + 10	7.15E + 09	2.51E + 10
	$1D_{leaky}$:1D Ratio	1.859	0.894	1.664	1.301	2.135
Baseline CMVR	**1D**	2.82E + 10	3.32E + 10	1.735E + 10	9.19E + 09	3.49E + 10
	$1D_{leaky}$	5.95E + 10	9.34E + 10	2.974E + 10	1.59E + 10	7.12E + 10
	$1D_{leaky}$:1D Ratio	1.927	0.704	1.799	1.414	2.316

diagnostic and quantitative metrics (see Table 2). Mean bias of vFFR was similar between 1D and $1D_{leaky}$ models (0.06(0.00–0.10) vs 0.07(0.00–0.11), p = 0.08). The $1D_{leaky}$ model had greater absolute error than the 1D model (0.08(0.04–0.13) vs 0.08(0.04–0.14), p = 0.02). Fig. 2B–D shows Bland-Altman plots for each model.

3.4. Hyperaemic flow computation

Inflow and outflow for each model were compared (Figs. 3 and 4). The $1D_{leaky}$ model inflow was significantly higher (1.97(1.13–3.45) mL/s or 148%(125–190%) of 1D flow, p ≤ 0.001) and outflow was significantly lower (0.75(0.36–1.35) mL/s or 60%(47–77%) of

Table 5
Comparison of model predicted hyperaemic inflows Q^{Hyp} with flows measured by Xaplanteris et al. (Xaplanteris et al., 2018) via thermodilution. (All values in mL/s).

	LAD			LCX			RCA		
	1D	$1D_{leaky}$	Thermo.	1D	$1D_{leaky}$	Thermo.	1D	$1D_{leaky}$	Thermo.
25th percentile	0.89	1.50	2.52	0.51	0.87	2.00	0.49	0.63	1.97
Median	1.59	2.41	3.15	1.07	1.76	2.47	0.88	1.24	2.77
75th percentile	2.24	3.80	3.87	1.60	2.97	3.27	1.53	2.03	3.50
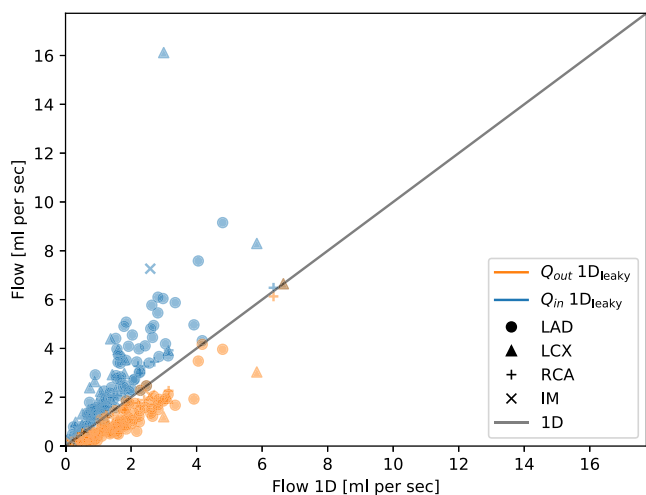
Fig. 3. Comparison of estimated hyperaemic flows between the models, Computed hyperaemic flow values are compared for each case studied. The 1D flow values are shown on the x axis and the $1D_{leaky}$ values on the y axis. The blue markers represent the $1D_{leaky}$ inflow and the orange markers represent the $1D_{leaky}$ outflow. The marker shape indicates the anatomical location of each case. The solid line represents the expected flow if both approaches agree. (For interpretation of the references to colour in this figure legend, the reader is referred to the web version of this article.)

1D flow, p < 0.001) compared to the 1D model (1.26(0.73–2.03)mL/s. The median artery leaked 63%(44–74%) of flow (1.09(0.40–2.09) mL/s) between inlet and outlet, and including leakage increased inflow 0.63(0.19–1.18) mL/s and decreased outflow 0.46(0.18–0.77) mL/s.

3.5. Baseline flow and coronary flow reserve

Baseline volumetric flows were computed for 107 vessels for which baseline pressure recordings were available and showed a difference greater than 133.32 Pa. The baseline inflows for the $1D_{leaky}$ model (1.05(0.49–1.94) mL/s) were significantly higher compared to the 1D model (0.64(0.31–1.24) mL/s; p < 0.001). No significant difference in the coronary flow reserve (CFR) predicted by matching measured pressures was found (1D_leaky 1.92(1.54–2.62) vs 1D 1.92(1.54–2.59), p = 0.236); however, the vCFR predicted in the same manner as vFFR differed significantly (1Dleaky 2.91(2.42–3.09) vs 1D 2.74(2.36–2.93), p < 0.001) with a 95% confidence interval of (0.136, 0.176) for the mean difference between the models (see Fig. 5).

3.6. Stenotic and myocardial resistances

1D segment resistance (SR) was lower than for 1Dleaky (3.17e+09 ± 5.9e+09 vs $1D_{leaky}$ 3.19e+09 ± 7.0e+09 Pa/m^3 s^{-1}, a ratio of 0.91, p < 0.001). $1D_{leaky}$ hyperaemic CMVR was significantly higher (1D 6.93e+09(4.49e+09–1.25e+10) vs $1D_{leaky}$ 1.25e+10(7.15e+09–2.51e+10) Pa/m^{3}s^{-1} a ratio of 1.86 of 1D, p ≤ 0.001).

4. Discussion

We analysed the importance of accounting for flow to coronary arterial side branches upon computed FFR and measures of flow in the main vessel. We implemented a computational model in which a leakage function mimicked the flow to branches. Accuracy of computed FFR was unaffected by the presence of branches, whereas inlet volumetric flow increased and was more similar to hyperaemic values (see Table 5 and Xaplanteris et al. (2018)). The still somewhat lower value of flow found for the $1D_{leaky}$ model may be partly explained by the fact that FFR in the current population was lower.

Thus, compensating for side-branch flow does not appear to improve the prediction of FFR but is an important consideration when estimating flow rate and associated indices such as predicted CFR.

4.1. FFR computation

Several proposed methods of FFR computation achieve reasonable diagnostic accuracy in determining whether FFR is ≤ or > 0.80; however, quantitative accuracy is limited. For models of vFFR the limits of agreement are in the order of ±0.15(Morris et al., 2015). Considering the range for intermediate vessels (0.70–0.90), this makes interpretation of individual results difficult. All methods neglect some side branches either explicitly or due to limited image resolution. We hypothesised that accounting for branch flow with the proposed leakage model could improve vFFR estimation but found this not to be the case. Addition of a leakage function to a 1D model increased vFFR by an average of 0.005 and did not affect accuracy (see Fig. 2 and Table 2).

FFR depends upon inflow to the coronary vasculature, the relative resistances of all branches, and the CMVR. Direct measurement of FFR accounts for impacts of side branches, visible or not; whereas vFFR often ignores them or only incorporates the larger ones. Configuration of model boundary conditions may compensate for this to a degree. In our model, the inlet is defined as the proximal aortic pressure and the outlet by a generic, model-specific resistance value representing the CMVR and tuned to the model, but not to the individual patient. Determination of patient specific CMVR requires a pressure wire in the distal position. Lower outflow in the $1D_{leaky}$ model compared with the 1D model results in a higher average CMVR, which effectively tunes the boundary condition to achieve similar predictive accuracy for FFR. Thus the tuning of boundary conditions may obviate differences in predicted FFR that are expected if models predict flows quite different from the unknown physical flow. Moreover, as FFR depends upon the relative pressures, as a proxy for relative flow, the value of predicted FFR can be identical for models with different volumetric flows.

Our finding that vFFR is unaffected by branch flow contrasts with previous studies(Li et al., 2015; Sturdy et al., 2019; Vardhan et al., 2019). Li et al. (2015) compared haemodynamic indices predicted by single lumen models and full tree models derived from fusion of optical coherence tomography and 3D coronary angiography and found that P_d/P_a increased by an average of 0.06
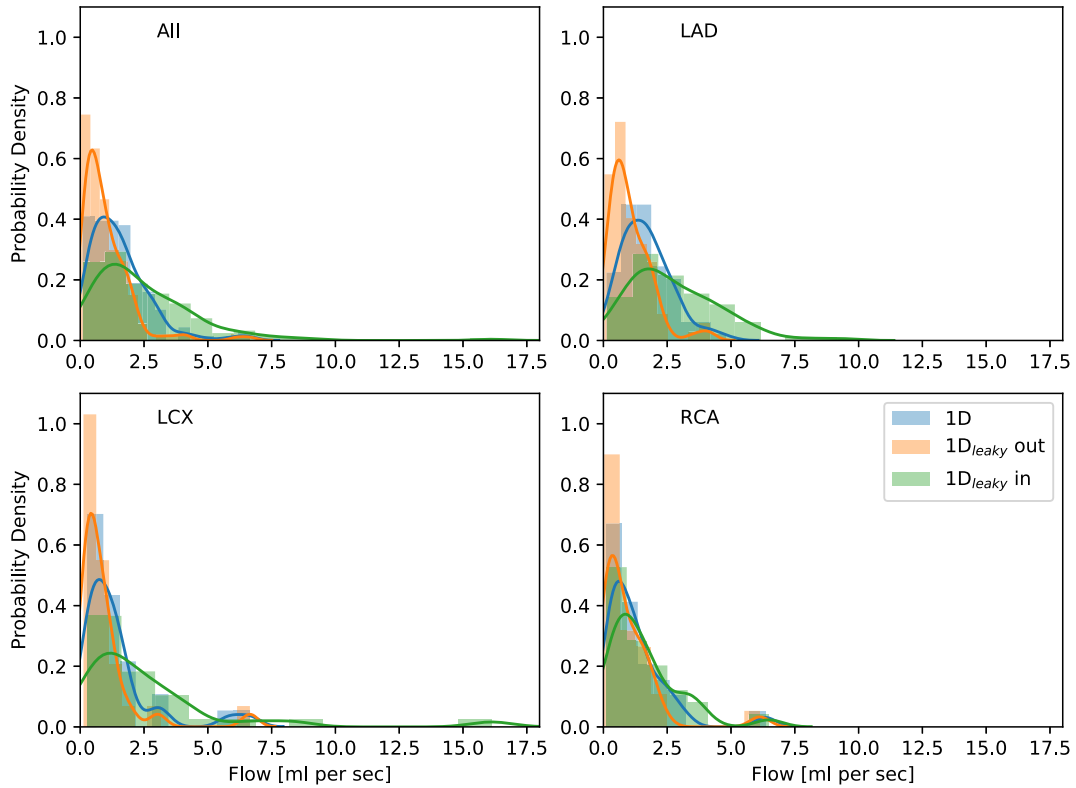
Fig. 4. Computed hyperaemic flows for both models, The overall distribution of hyperaemic inflow and outflow is shown for each model, with estimated probability density shown as a line. The first panel (All) shows the distribution over all studied arteries, while subsequent panels display the distribution of arteries of specific branch type (LAD, RCA or LCX). In the conventional 1D model inflow and outflow are identical.
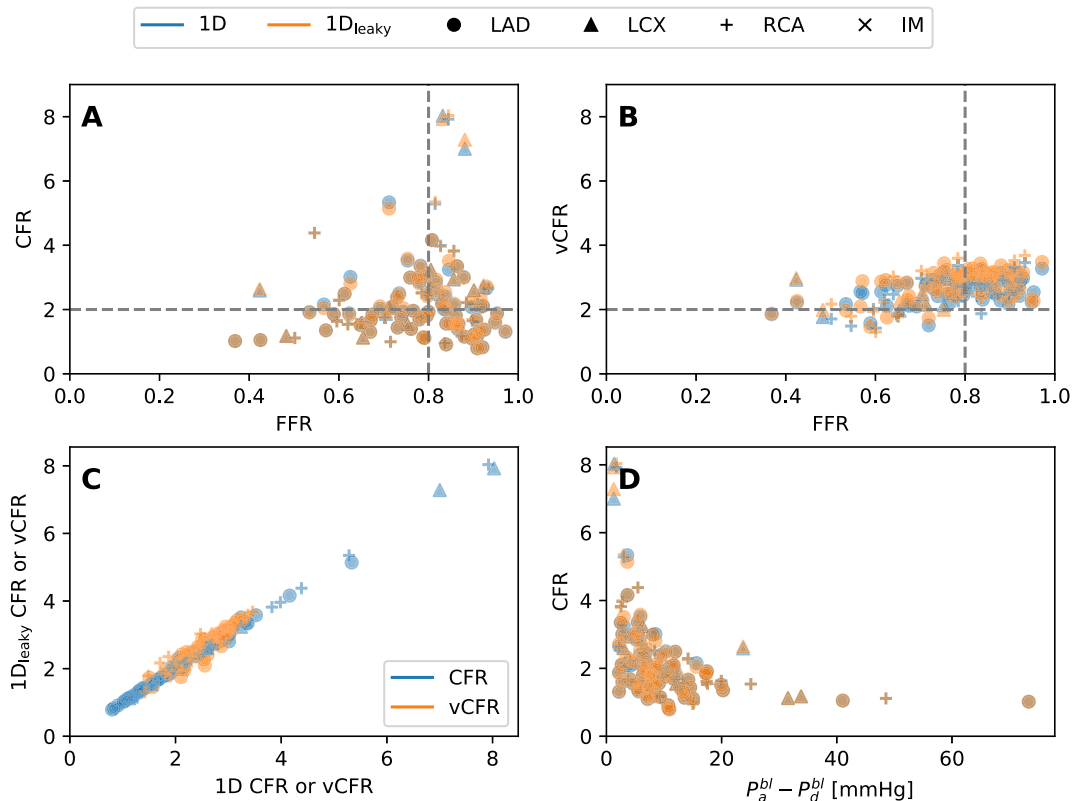
Fig. 5. Comparison of CFR, vCFR, FFR and baseline pressures, CFR derived from invasive pressures (A) and vCFR based on average CMVR (B) plotted against measured FFR. The dashed lines represent the clinical cut off points; FFR = 0.80 and CFR = 2.0. (C) The $1D_{leaky}$ CFR (blue) or vCFR (orange) plotted against 1D CFR or vCFR. (D) Predicted CFR plotted against the measured pressure difference (P_a-P_d) at baseline conditions suggests the sensitivity of CFR estimates to variations of pressure when P_a-P_d is small. (For interpretation of the references to colour in this figure legend, the reader is referred to the web version of this article.)

(p $\leq$ 0.001) in the full tree model. Sturdy et al. (2019) reported significant changes in vFFR using a full tree model with branches down to diameter of 0.1 mm compared to a model neglecting branches with diameter < 1 mm. Vardhan et al. (2019) demonstrated that neglecting side branches increased estimates of wall shear stresses in coronary trees of 21 patients by comparing 3D CFD of geometries reconstructed from biplane angiography images and including all, some and no side branches. These previous studies all found significant changes in pressure drops when imposing fixed inflow conditions on models accounting for varying numbers of branches.

The difference between these results and the marginal change we found in vFFR of the 1D$_{leaky}$ model (0.005) is due to differences in the imposed boundary conditions. As prior approaches imposed the same inlet flow rate in both the single lumen (or reduced branching) and the tree model, the single lumen model will have relatively more flow through the same vessel, resulting in a smaller Pd/Pa. As the pressure drop directly results from the flow through a given artery, imposing a specific flow will result in elevated flow in single lumen models relative to branched models and thus directly affect vFFR. In contrast the pressure and resistance boundary conditions in the present study (and their tuning for the respective modelling approaches) allow the flow to vary to match the model geometry, measured arterial pressure and model resistance. Thus, while in both cases the pressure drop is directly linked to the flow, the present procedure for computing vFFR may be less affected by accounting for flow to side branches than approaches that impose flow.

The fact that the importance of including leakage terms appears to be related to the choice of boundary conditions is relevant when considering which modelling approach to employ for predicting FFR. The importance of accurate boundary conditions for prediction of FFR is well known. For example, significant individual variability of terminal resistances, CMVR, is known to be a primary source of uncertainty in predicting FFR (Morris et al., 2015) (Supplemental Fig. 1 shows that error in vFFR increases as the CMVR is further from R_{model}).

4.2. Computation of flow

Whilst FFR prediction was unaffected by compensation for side-branch flow, significant differences in computed flow rates were observed (Figs. 3 and 4). The leakage function increased average inlet hyperaemic flow from 1.53 mL/s to 2.52 mL/s, (65% increase) and decreased outlet flow from 1.53 mL/s to 1.00 mL/s (35% decrease). On average, 56% of flow leaked from inlet to outlet. This phenomenon was highest in LAD arteries (60%) and lowest in the RCA (44%) as hypothesized and directly resulting from the more significant tapering of LAD arteries relative to non-LAD arteries (see Table 1 and supplementary material); however, accuracy of vFFR was similar for LAD and non-LAD arteries. Li et al. (2015) also found the flow reduction to be greatest in LAD arteries and observed a similar reduction in outlet flow (from 1.89 mL/s to 1.38 mL/s). The flows predicted by the 1Dleaky model more closely resemble those measured by thermodilution (see Table 5 and Xaplanteris et al., 2018). Some discrepancy between the predicted flows and those measured by thermodilution may be explained by the relatively lower FFR in the present population.

4.3. The difference between FFR and volumetric blood flow

In the presence of side branches, coronary inlet flow will always exceed outlet flow. The 1Dleaky model accounts for this effect and quantifies flow lost from the main vessel to the side branches. However, despite significant differences in coronary flow rates, FFR was unaffected. Why is FFR, an index of coronary flow, agnostic to changes in flow? FFR is a surrogate index, derived from a ratio of invasively measured pressures. FFR reports the *ratio* of flow in the diseased artery relative to the hypothetical flow (an unknown value) that would occur in the healthy artery. FFR is therefore unable to predict volumetric flow and, given an unchanged ratio of pressures, FFR will be similarly unchanged.

Van de Hoef et al. (2014) demonstrated discordance in FFR and CFR results in 37% of cases. In our study, the range of computed CFR was larger than that found by Van de Hoef et al. (0.8–8.0 vs 1.0–5.5) which may be explained by uncertainties in the measured pressure drops for cases where the pressure drop at baseline was small (see Fig. 5D). The computed CFR was discordant from measured FFR in 42% of cases for both approaches (Fig. 5A). For individuals with discordant results, CFR has been found to be a better predictor of long term prognosis than FFR (Echavarria-Pinto et al., 2013). The ability to combine a measure of volumetric flow with FFR might add value when assessing patients with CAD.

4.4. Limitations

The accuracy of computed FFR results are affected by the accuracy of the reconstruction and assumptions about the boundary conditions. The generic resistance applied at the distal boundary when computing vFFR limits case-specific accuracy. Further, since this resistance was calibrated using all cases, the predictive accuracy may be worse if this value is applied to future cases. However, the same assumptions were made in each model, allowing accurate between-model comparison; the primary aim of this study. The clinical data were obtained under ideal circumstances in elective cases; however, no invasive flow measurements were acquired for comparison of computed flow values. Without flow measurements, comparison with previous studies is complicated and individual accuracy is unknown. A lack of information about larger side branches prohibits direct comparison of the leakage model with models that explicitly include side branches. The assumption that vessel taper corresponds to flow to side branches neglects the possibility that taper may reflect the presence of concentric atheroma, which may invalidate Murray's law. Some 1D$_{leaky}$ inflows are unphysiologically large (e.g. 17.5 mL/s), which likely occurs when taper does not correspond to Murray's law. Stenoses at the inlet of the artery and tapering due to disease may both cause the tapering ratio to misrepresent the flow to side branches, an appropriate methodology to identify abnormal taper from healthy taper would be valuable in further investigations. Further, flow to side branches is likely distributed non-uniformly and a leakage model accounting for variations could be explored.

Side branch flow likely affects diffuse lesions differently than focal lesions; however, as the data are not annotated to differentiate these cases, this hypothesis was not evaluated. Further, the heuristic stenosis detection algorithm purports to identify regions where the 1D assumptions are violated and thus may not necessary mark all diseased regions or may break the diseased region into multiple regions. Comparison of stenotic flow between models would require an appropriate method to define which flow should be compared between the models. The segment resistance, defined based on average flow, provides one point of comparison.

5. Conclusion

The accuracy of computational models of FFR depends on the anatomical and physiological assumptions which are made during the computational process. This study tested the assumption that coronary physiology can be accurately predicted using computational models that neglect side-branches. The addition of a leakage term had no significant effect on the predictive accuracy of vFFR despite significant differences in the estimated volumetric flow rate. The insensitivity of accuracy of predicted vFFR to differences

in predicted flow may reflect the fact that FFR is a ratio whereas absolute measures of flow will be directly affected. The increasing adoption of computed physiological indices may require better understanding of the significance of both relative and absolute measures of coronary artery function.

Funding

Declaration of Competing Interest

The authors declare that they have no known competing financial interests or personal relationships that could have appeared to influence the work reported in this paper.

Appendix A. Supplementary data

Supplementary data to this article can be found online at https://doi.org/10.1016/j.jbiomech.2020.109698.

References

Alastruey, J., Xiao, N., Fok, H., Schaeffter, T., Figueroa, C.A., 2016. On the impact of modelling assumptions in multi-scale, subject-specific models of aortic haemodynamics. J. R. Soc. Interface 13, 20160073.

Blanco, P.J., Bulant, C.A., Muller, L.O., Talou, G.D.M., Bezerra, C.G., Lemos, P.A., Feijoo, R.A., 2018. Comparison of 1D and 3D models for the estimation of fractional flow reserve. Sci. Rep. 8, 17275.

Boileau, E., Nithiarasu, P., Blanco, P.J., Müller, L.O., Fossan, F.E., Hellevik, L.R., Donders, W.P., Huberts, W., Willemet, M., Alastruey, J., 2015. A benchmark study of numerical schemes for one-dimensional arterial blood flow modelling. Int. J. Numer. Method Biomed. Eng. 31, e02732.

Dehmer, G.J., Weaver, D., Roe, M.T., Milford-Beland, S., Fitzgerald, S., Hermann, A., Messenger, J., Moussa, I., Garratt, K., Rumsfeld, J., Brindis, R.G., 2012. A contemporary view of diagnostic cardiac catheterization and percutaneous coronary intervention in the United States: a report from the CathPCI Registry of the National Cardiovascular Data Registry, 2010 through June 2011. J. Am. Coll. Cardiol 60, 2017–2031.

Echavarria-Pinto, M., Escaned, J., Macias, E., Medina, M., Gonzalo, N., Petraco, R., Sen, S., Jimenez-Quevedo, P., Hernandez, R., Mila, R., Ibanez, B., Nunez-Gil, I.J., Fernandez, C., Alfonso, F., Banuelos, C., Garcia, E., Davies, J., Fernandez-Ortiz, A., Macaya, C., 2013. Disturbed coronary hemodynamics in vessels with intermediate stenoses evaluated with fractional flow reserve: a combined analysis of epicardial and microcirculatory involvement in ischemic heart disease. Circulation 128, 2557–2566.

Eck, V.G., Donders, W.P., Sturdy, J., Feinberg, J., Delhaas, T., Hellevik, L.R., Huberts, W., 2016. A guide to uncertainty quantification and sensitivity analysis for cardiovascular applications. Int. J. Numer. Method. Biomed. Eng. 32.

Fossan, F.E., Sturdy, J., Muller, L.O., Strand, A., Braten, A.T., Jorgensen, A., Wiseth, R., Hellevik, L.R., 2018. Uncertainty quantification and sensitivity analysis for computational FFR estimation in stable coronary artery disease. Cardiovasc. Eng. Technol. 9, 597–622.

Gosling, R.C., Morris, P.D., Soto, D.A.S., Lawford, P.V., Hose, D.R., Gunn, J.P., 2019. Virtual coronary intervention: a treatment planning tool based upon the angiogram. JACC: Cardiovasc. Imaging 12 (5), 865–872. https://doi.org/10.1016/j.jcmg.2018.01.019.

Koo, B.K., Erglis, A., Doh, J.H., Daniels, D.V., Jegere, S., Kim, H.S., Dunning, A., DeFrance, T., Lansky, A., Leipsic, J., Min, J.K., 2011. Diagnosis of ischemia-causing coronary stenoses by noninvasive fractional flow reserve computed from coronary computed tomographic angiograms. Results from the prospective multicenter DISCOVER-FLOW (Diagnosis of Ischemia-Causing Stenoses Obtained Via Noninvasive Fractional Flow Reserve) study. J. Am. Coll. Cardiol. 58, 1989–1997.

Li, Y., Gutierrez-Chico, J.L., Holm, N.R., Yang, W., Hebsgaard, L., Christiansen, E.H., Maeng, M., Lassen, J.F., Yan, F., Reiber, J.H., Tu, S., 2015. Impact of side branch modeling on computation of endothelial shear stress in coronary artery disease:

coronary tree reconstruction by fusion of 3D angiography and OCT. J. Am. Coll Cardiol 66, 125–135.

Liang, F., Fukasaku, K., Liu, H., Takagi, S., 2011. A computational model study of the influence of the anatomy of the circle of willis on cerebral hyperperfusion following carotid artery surgery. Biomed Eng Online 10, 84.

Min, J.K., Leipsic, J., Pencina, M.J., Berman, D.S., Koo, B.K., van Mieghem, C., Erglis, A., Lin, F.Y., Dunning, A.M., Apruzzese, P., Budoff, M.J., Cole, J.H., Jaffer, F.A., Leon, M. B., Malpeso, J., Mancini, G.B., Park, S.J., Schwartz, R.S., Shaw, L.J., Mauri, L., 2012. Diagnostic accuracy of fractional flow reserve from anatomic CT angiography. JAMA 308, 1237–1245.

Morris, P.D., Curzen, N., Gunn, J.P., 2020. Angiography-derived fractional flow reserve: more or less physiology?. J. Am. Heart Assoc. https://doi.org/10.1161/JAHA.119.015586. In press.

Morris, P.D., Ryan, D., Morton, A.C., Lycett, R., Lawford, P.V., Hose, D.R., Gunn, J.P., 2013. Virtual fractional flow reserve from coronary angiography: modeling the significance of coronary lesions: results from the VIRTU-1 (VIRTUal Fractional Flow Reserve From Coronary Angiography) study. JACC Cardiovasc. Interv. 6, 149–157.

Morris, P.D., Silva Soto, D.A., Feher, J.F.A., Rafiroiu, D., Lungu, A., Varma, S., Lawford, P.V., Hose, D.R., Gunn, J.P., 2017. Fast virtual fractional flow reserve based upon steady-state computational fluid dynamics analysis: results from the VIRTU-fast study. JACC Basic Transl. Sci. 2, 434–446.

Morris, P.D., van de Vosse, F.N., Lawford, P.V., Hose, D.R., Gunn, J.P., 2015. "Virtual" (Computed) fractional flow reserve: current challenges and limitations. JACC Cardiovasc. Interv. 8, 1009–1017.

Murray, C.D., 1926. The physiological principle of minimum work: I. The vascular system and the cost of blood volume. Proc. Natl. Acad. Sci. USA 12, 207–214.

Nakazato, R., Park, H.B., Berman, D.S., Gransar, H., Koo, B.K., Erglis, A., Lin, F.Y., Dunning, A.M., Budoff, M.J., Malpeso, J., Leipsic, J., Min, J.K., 2013. Noninvasive fractional flow reserve derived from computed tomography angiography for coronary lesions of intermediate stenosis severity: results from the DeFACTO study. Circ. Cardiovasc. Imaging 6, 881–889.

Neumann, F.J., Sousa-Uva, M., Ahlsson, A., Alfonso, F., Banning, A.P., Benedetto, U., Byrne, R.A., Collet, J.P., Falk, V., Head, S.J., Juni, P., Kastrati, A., Koller, A., Kristensen, S.D., Niebauer, J., Richter, D.J., Seferovic, P.M., Sibbing, D., Stefanini, G.G., Windecker, S., Yadav, R., Zembala, M.O., Group, E.S.C.S.D., 2018. 2018 ESC/EACTS Guidelines on myocardial revascularization. Eur. Heart J.

Norgaard, B.L., Leipsic, J., Gaur, S., Seneviratne, S., Ko, B.S., Ito, H., Jensen, J.M., Mauri, L., De Bruyne, B., Bezerra, H., Osawa, K., Marwan, M., Naber, C., Erglis, A., Park, S. J., Christiansen, E.H., Kaltoft, A., Lassen, J.F., Botker, H.E., Achenbach, S., N, X. T. Trial Study Group, 2014. Diagnostic performance of noninvasive fractional flow reserve derived from coronary computed tomography angiography in suspected coronary artery disease: the NXT trial (Analysis of Coronary Blood Flow Using CT Angiography: Next Steps). J. Am. Coll. Cardiol. 63, 1145–1155.

Papafaklis, M.I., Muramatsu, T., Ishibashi, Y., Lakkas, L.S., Nakatani, S., Bourantas, C. V., Ligthart, J., Onuma, Y., Echavarria-Pinto, M., Tsirka, G., Kotsia, A., Nikas, D.N., Mogabgab, O., van Geuns, R.J., Naka, K.K., Fotiadis, D.I., Brilakis, E.S., Garcia-Garcia, H.M., Escaned, J., Zijlstra, F., Michalis, L.K., Serruys, P.W., 2014. Fast virtual functional assessment of intermediate coronary lesions using routine angiographic data and blood flow simulation in humans: comparison with pressure wire – fractional flow reserve. EuroIntervention 10, 574–583.

Sankaran, S., Kim, H.J., Choi, G., Taylor, C.A., 2016. Uncertainty quantification in coronary blood flow simulations: impact of geometry, boundary conditions and blood viscosity. J. Biomech. 49, 2540–2547.

Sciola, M.I., Morris, P.D., Gosling, R., Lawford, P.V., Hose, D.R., Gunn, J.P., 2018. The impact of Objective Mathematical Analysis during Fractional Flow Reserve measurement: results from the OMA-FFR study. EuroIntervention 14, 935–941.

Seabold, S., Perktold, J., 2010 Statsmodels: Econometric and statistical modeling with python. In: Proceedings of the 9th Python in Science Conference.

Sturdy, J., Kjernlie, J.K., Nydal, H.M., Eck, V.G., Hellevik, L.R., 2019. Uncertainty quantification of computational coronary stenosis assessment and model based mitigation of image resolution limitations. J. Computat. Sci. 31, 137–150.

Tu, S., Barbato, E., Koszegi, Z., Yang, J., Sun, Z., Holm, N.R., Tar, B., Li, Y., Rusinaru, D., Wijns, W., Reiber, J.H., 2014. Fractional flow reserve calculation from 3-dimensional quantitative coronary angiography and TIMI frame count: a fast computer model to quantify the functional significance of moderately obstructed coronary arteries. JACC Cardiovasc. Interv. 7, 768–777.

Tu, S., Westra, J., Yang, J., von Birgelen, C., Ferrara, A., Pellicano, M., Nef, H., Tebaldi, M., Murasato, Y., Lansky, A., 2016. Diagnostic accuracy of fast computational approaches to derive fractional flow reserve from diagnostic coronary angiography: the international multicenter FAVOR pilot study. JACC: Cardiovascular Interventions 9, 2024–2035.

van de Hoef, T.P., van Lavieren, M.A., Damman, P., Delewi, R., Piek, M.A., Chamuleau, S.A.J., Voskuil, M., Henriques, J.P.S., Koch, K.T., de Winter, R.J., et al., 2014. Physiological basis and long-term clinical outcome of discordance between fractional flow reserve and coronary flow velocity reserve in coronary stenoses of intermediate severity. Circinterventions 113, 1049.

Vardhan, M., Gounley, J., Chen, S.J., Kahn, A.M., Leopold, J.A., Randles, A., 2019. The importance of side branches in modeling 3D hemodynamics from angiograms for patients with coronary artery disease. Sci. Rep. 9, 8854.

Xaplanteris, P., Fournier, S., Keulards, D.C.J., Adjedj, J., Ciccarelli, G., Milkas, A., Pellicano, M., Van't Veer, M., Barbato, E., Pijls, N.H.J., De Bruyne, B., 2018. Catheter-based measurements of absolute coronary blood flow and microvascular resistance: feasibility, safety, and reproducibility in humans. Circ. Cardiovasc. Interv. 11, e006194.